Title
Laser Fabrication of Two-Dimensional Rotating-Lattice Single Crystal

Journal
Crystal Growth & Design, 17(4)

ISSN
1528-7483

Authors
Savytskii, Dmytro
Au-Yeung, Courtney
Dierolf, Volkmar
et al.

Publication Date
2017-04-05

DOI
10.1021/acs.cgd.6b01709

Peer reviewed

Laser fabrication of 2D rotating-lattice single crystal

Journal:	*Crystal Growth & Design*
Manuscript ID	Draft
Manuscript Type:	Article
Date Submitted by the Author:	n/a
Complete List of Authors:	Savytskyy , Dmytro; Lehigh University, Jain, Himanshu; Lehigh University, Materials Science and Engineering Department Au-Yeung, Courtney; Lehigh University, Physics Department Dierolf, Volkmar; Lehigh University, Physics Tamura, Nobumichi; Lawrence Berkeley National Lab, Advanced Light Source

Laser fabrication of 2D rotating-lattice single crystal

Dmytro Savytskii[1], *Himanshu Jain*[1]*, *Courtney Au-Yeung*[2], *Volkmar Dierolf*[2], *Nobumichi Tamura*[3]

[1]Materials Science and Engineering Department, Lehigh University, 5 East Packer Avenue, Bethlehem, PA 18015, USA

[2]Physics Department, Lehigh University, 16 Memorial Drive East, Bethlehem, PA 18015, USA

[3]Lawrence Berkeley National Laboratory, Berkeley, CA, 94720, USA

Abstract:

A rotating lattice single (RLS) crystal is a unique form of solid, which was fabricated recently as a 1D architecture in glass via solid state transformation induced by laser irradiation. In these objects, the lattice rotates gradually and predictably about an axis that lies in the plane of the line and is normal to the laser scanning direction. This paper reports the fabrication of Sb_2S_3 2D RLS crystals on the surface of $16SbI_3$–$84Sb_2S_3$ glass: individual RLS crystal lines are joined together using 'stitching' or 'rastering' as two successful protocols. The electron back scattered diffraction (EBSD) mapping and scanning Laue X-ray microdiffraction (μSXRD) of the 2D RLS crystals show gradual rotation of lattice comprising of two components, one along the length of each line and another normal to this direction. The former component is determined by the rotation of the first line of the 2D pattern, but the relative contribution of the last component depends on the extent of overlap between two successive lines. By appropriate choice of initial seed orientation and the direction of scanning it is possible to control the lattice rotation, even reduce it down to ~5° for a 50x50 μm^2 2D pattern of Sb_2S_3 crystal.

Figure:

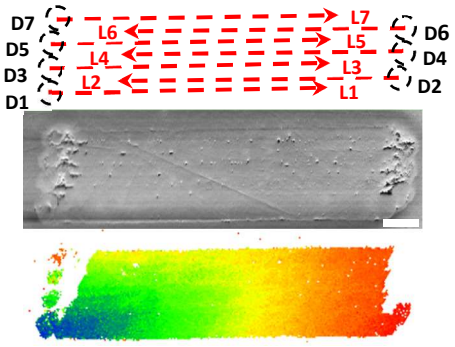

***Corresponding author:**

Himanshu Jain

Materials Science and Engineering Department

Lehigh University,

5 East Packer Avenue

Bethlehem, PA 18015, USA

Phone: 1-610-758-4217. Fax: 1-610-758-4244.

E-mail: h.jain@Lehigh.EDU

Web: http://www.lehigh.edu/~inmatsci/faculty/jain/jain.htm

Laser fabrication of 2D rotating-lattice single crystal

Dmytro Savytskii[1], Himanshu Jain[1], Courtney Au-Yeung[2], Volkmar Dierolf[2], Nobumichi Tamura[3]*

[1]Materials Science and Engineering Department, Lehigh University, 5 East Packer Avenue, Bethlehem, PA 18015, USA

[2]Physics Department, Lehigh University, 16 Memorial Drive East, Bethlehem, PA 18015, USA

[3]Lawrence Berkeley National Laboratory, 1 Cyclotron Road, Berkeley, CA, 94720, USA

ABSTRACT

A rotating lattice single (RLS) crystal is a unique form of solid, which was fabricated recently as 1D architecture in glass via solid state transformation induced by laser irradiation. In these objects, the lattice rotates gradually and predictably about an axis that lies in the plane of the line and is normal to the laser scanning direction. This paper reports the fabrication of Sb_2S_3 2D RLS crystals on the surface of $16SbI_3$–$84Sb_2S_3$ glass: individual RLS crystal lines are joined together using 'stitching' or 'rastering' as two successful protocols. The electron back scattered diffraction (EBSD) mapping and scanning Laue X-ray microdiffraction (μSXRD) of the 2D RLS crystals show gradual rotation of lattice comprising of two components, one along the length of each line and another normal to this direction. The former component is determined by the rotation of the first line of the 2D pattern, but the relative contribution of the last component depends on the extent of overlap between two successive lines. By appropriate choice of initial

seed orientation and the direction of scanning it is possible to control the lattice rotation, even reduce it down to ~5^{o} for a 50x50 μm^2 2D pattern of Sb_2S_3 crystal.

INTRODUCTION

Laser-induced crystallization of glass has become a viable method for fabricating single crystals of complex oxides[1-4], chalcogenides[5-7], etc., especially when the goal is a crystal of complex shape and small dimensions. Typically, the laser is used to heat the glass locally to initiate nucleation and form a seed crystal, which is then grown into a single crystal line via controlled displacement of the sample relative to laser. The process yields single-crystal architecture in glass (SCAG) comprising of straight and curved lines. A continuous wave (CW) laser of suitable wavelength is used to create SCAG at or near the surface[1, 4-7], whereas femtosecond (fs) laser can yield SCAG in 3D deep inside the glass[2,3]. In either case, the glass generally melts at the focal point of the laser and crystal forms as the melt solidifies. Single crystallinity of the structure is assured by the fact that the crystal grows preferentially in a specific direction and that there is a steep temperature gradient provided by the relatively fast movement of the laser from seed onward.

Having established the process for fabricating zero dimensional single crystal dots and 1D single crystal lines, the application space of the method is significantly enhanced when individual lines are merged to form 2D planar structures on the surface of glass as demonstrated by Komatsu's group at Nagaoka University[8-10]. It fabricated 'highly oriented' 2D crystal patterns of $LiNbO_3$, β-BaB_2O_4, and β'-$Gd_2(MoO_4)_3$, within intrinsically simple silicate or borate glass matrix, where laser induced crystal growth occurs from the melt. The 2D patterns were created as array of lines with a small step between them. That is, a laser-induced line was made to overlap with a previously laser-written. However, the truly single-crystal nature of such patterns

has remained to be confirmed. For $LiNbO_3$ they showed by polarized micro-Raman spectra and second harmonic signal intensity that the crystal's *c*-axis was always along the laser scanning direction when forming the 2D pattern[8]. However, different results were obtained for the 2D patterns of β-BaB_2O_4 and β'-$Gd_2(MoO_4)_3$ crystals[9,10]. In these cases, the lattice of the first crystal line changed its orientation so that in the final part of the pattern the crystal lattice had orientation perpendicular to the initial line orientation. Thus, under certain conditions the initial crystal may not act as the seed of subsequent crystal lines. The reason for this switching of lattice orientation remains unclear.

A remarkable feature of laser-induced single crystal growth is that not only one can obtain single crystal starting from the melt, as mentioned above, but also by the heating of a glass to its crystallization temperature (T_x)[7]. This all-solid state single crystal formation contrasts devitrification of glass to form glass-ceramics that inevitably comprise of a very large number of fine grains resulting from spontaneous nucleation at multiple locations in the sample. It has opened the possibility of fabricating single crystals of complex compositions that could not be done before, such as the ones that melt incongruently, or decompose/undergo undesirable phase transformation upon heating beyond Tx to the melting temperature (Tm). In this method, the growing crystal is surrounded by solid glass. Since the molar volume of glass is often larger than that of the corresponding crystal, the growth of new crystal occurs necessarily in the presence of stress. When the crystal is grown on the surface such as by heating with a CW laser, the stress is anisotropic. Consequently, the lattice of the single crystal lines 'written' on the surface of glass has unique structure, exhibiting gradual rotation of crystal orientation[11]. For example, the orientation of unit cell of the single crystal line of Sb_2S_3 fabricated by CW laser heating on the surface of an Sb-S-I glass gradually changes as one moves along the laser scanning direction.

Specifically, the lattice rotates downwards about the axis that is in the plane of crystal, which is also the sample surface, and normal to the direction of laser scanning. Such a laser-written line constitutes a special form of single crystals, which have been labeled as 'rotating lattice single' (RLS) crystals[11]. An RLS crystal has translational periodicity of a unit cell but only in one direction, which is normal to the laser scan direction and parallel to glass surface. For the two other normal space directions, the translation symmetry is broken by an ordered dislocations system.

In general, a 2D single crystal layer may be created as array of lines with a small step between them, so that a previously formed line acts as the seed for the growth of the new line. There must not be any other competing nucleation, but only the growth from the preceding line. Whereas this appears plausible, at least in principle, the rotation of lattice within an RLS crystal line introduces new challenges for joining such lines to obtain a 2D RLS crystal layer. Figure 1 illustrates the situation with two scenarios of crystal growth schematically: First a 1D RLS crystal line is formed by scanning the laser beam in x-direction. The orientation of lattice, θ, as defined by the angle between the direction of the normal to surface lattice plane at the beginning of the line and the same plane at the position of interest, varies with x. Experiments have shown that for a straight line θx varies linearly with x, which is the direction of laser displacement as well as the crystal growth[11]. After the first RLS crystal line has been fabricated to desired length, the next line must be formed, using the first line as the seed, by some small laser displacement and crystal growth in the y-direction and then scanning the laser in $-x$ direction. If the lattice rotates within the small segment along y-direction and then rotates during the growth in $-x$ direction, there will be a mismatch in the value of θy for the same value of x in the preceding and newly forming lines, and the two lines will join with constant θy misorientation. On the other

hand, if the new line grows from the preceding line at an angle to scanning direction, as the laser moves along –*x*-direction, there would appear an additional *y*-component of lattice rotation between the lines. This will be a non-ideal scenario for obtaining 2D RLS crystal layer, unless this component is sufficiently small (for instance, comparable to θx). When assessing these different possibilities, a crucial question arises: will the orientation of the lattice be determined by the direction of heat gradient (which will be predominantly along *x* direction) or the direction of crystal growth (which can have a component along *y*-direction)? Of course, if the rate of lattice rotation Θ (= θ °/μm) is different in *x* and –*x* directions, there could still be a seam between the lines and/or the nature of lattice rotation would become complex.

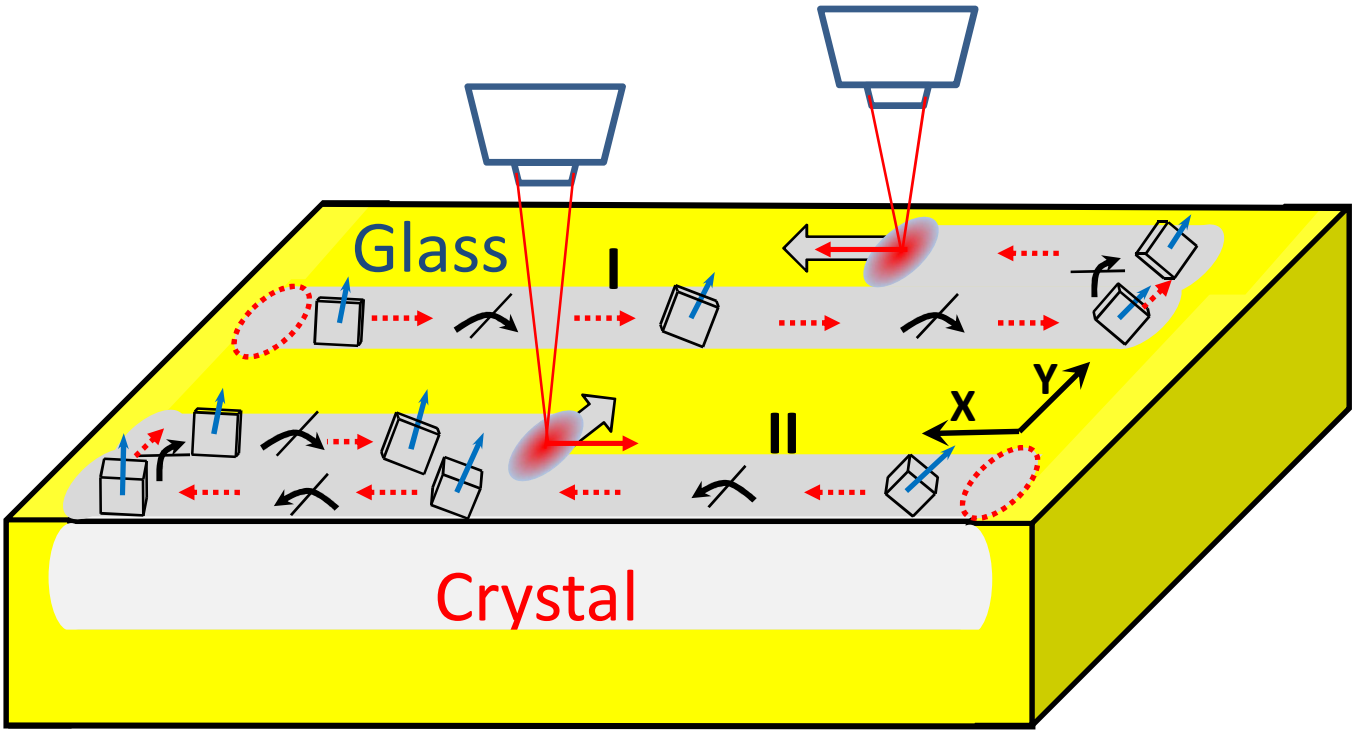

Figure 1. Two different growth scenarios for fabricating 2D laser-induced crystal, where the laser is scanned along x-axis along the length of the line, but along y-axis at the ends. In scenario (I) both the scanning and growth directions are parallel to each other, whereas in scenario (II) the growth direction is at an angle relative to the scanning direction.

The present study was motivated by the above issues, which are key to clarifying the nature of RLS crystals more generally as well as their potential for new applications. An indication of lattice rotation in 2D single crystal was mentioned recently[11], but its complete nature remains to be explored and understood. Toward this goal, our first task has been to determine if and how such a structure can be fabricated. The present study exploited the same Sb-S-I chalcogenide glass system for which 1D RLS crystal had been fabricated and characterized, wherein Sb_2S_3 crystal with unusual combination of superior ferroelectric and piezoelectric properties was formed[12].

EXPERIMENTAL

Design of crystallization protocols. Our experimental goal is to fabricate 2D RLS crystal layer on the surface of a glass in the shortest time possible. As mentioned above, toward this goal we must establish conditions that will allow fabrication of a broad 1D line of desired length, and then form subsequent lines using the preceding line as the seed; there should be no further independent nucleation. Two different protocols were designed to transform 1D single crystal lines into a 2D planar crystal: (a) Stitching protocol, and (b) Rastering protocol. The first protocol is a simple multiplication of the method that we used to produce 1D line[7]: At the beginning, a seed crystal is made by focusing the laser at some arbitrary spot from which the first crystal line is drawn subsequently. The laser is moved thereafter rapidly enough (for example, 20 μm/s), say in *x*-direction, the crystal grows without introducing additional nuclei. Thus the first 1D single crystal line is obtained and the process of crystallization is interrupted by switching off the laser beam after the desired length of the line is reached. To grow the next crystal lines needed to form 2D pattern, the sample is shifted in a direction orthogonal to the first line i.e. *y*-

direction by a few microns from the position at the end of the previous crystal and a new dot is formed to serve as the seed for growing the next line. All subsequent lines of the 2D pattern are created using the same three steps: 1) shifting in *y*-direction; 2) creating a new seed dot with short time exposure of the laser, and 3) growing from this seed the new crystal line. Here the laser-induced lines are made to overlap with the previously formed line and the above mentioned procedure of writing 1D line is repeated with the same experimental conditions except that the time exposure to form the second and subsequent seed dots (step 2) is reduced to a couple of seconds. This three-step process establishes the conditions for avoiding any new nucleation and crystal growth in *y*-direction while the laser is scanned along *x* (or –*x*) direction.

In the second protocol, a 2D crystal is made by "rastering" the laser beam continuously i.e. by traversing it without interrupting the irradiation when shifting the sample in the *y*-direction at the end of the line. Thus, a long serpentine line is created that consists of multiple long segments in *x*-direction with small *y*-steps between them, while keeping the same speed of translation in both (*x* and *y*) directions.

The difference between the 'stitching' and 'rastering' approaches arises from the way seed is formed at the beginning of individual crystal lines. In the first case, a seed grows from the end region of the previous crystal line, whereas in the latter case a crystal continuously grows under laser beam scanning, which bends twice by 90° between two successive lines (i.e. by making a U-turn). In other words, there is only one nucleation event in rastering. By comparison, in stitching protocol the number of nucleation events is the same as the number of lines to be stitched together. Thus rastering is a continuous writing process mimicking 'cursive writing' vs. 'printing' used in the 'stitching' protocol.

Glass Fabrication. The glass of non-stoichiometric $16SbI_3$-$84Sb_2S_3$ composition was made following the ampule quenching method, previously developed for the Sb-S-I system[6]. It was prepared from elemental powders of Sb, S, and I (>5N purity) using quartz ampules with 11 mm ID and 1 mm wall thickness. X-ray diffraction analysis of the as-quenched samples confirmed their amorphous state. The samples for laser treatment were polished to optical finish using metallographic techniques.

In order to obtain laser-induced crystallization of Sb_2S_3 phase, it was instructive to know how a given glass composition would transform upon simple heating. Therefore, usual temperature induced crystallization of $xSbSI$-$(100-x)Sb_2S_3$ pseudo-binary glass series was investigated in our group previously. It showed that for the glass of $16SbI_3$-$84Sb_2S_3$ composition Sb_2S_3 phase starts to crystallize first, in contrast to other compositions with higher concentration of iodine, where SbSI phase crystallized first at lower temperatures followed by Sb_2S_3. The presently selected glass composition still belongs to the glass forming region and can be synthesized without requiring unusually high quenching rates[13].

Laser heating. A fiber-coupled 639 nm diode laser (LP639-SF70, ThorLabs) was used to induce crystallization. Its intensity was controlled by a diode laser current controller (ILX Lightwave LDX-3545 Precision Current Source). The beam was focused on the polished surface of the glass sample by a 50x, 0.75NA microscope objective to a spot of a few μm diameter. Crystalline lines a few hundred μm long were fabricated by translating the sample at a fixed power density. To avoid oxidation, the sample was placed in a flowing nitrogen environment on a custom-built stage, which could be translated independently in the *x*-, *y*-, and *z*-directions. A CCD camera monitored the sample *in-situ*, while LabView software controlled the laser

intensity, and the movement of the stage. The optical setup and procedure for the fabrication of crystals has been described in detail in previous publications[14-16].

Characterization of crystallinity. The laser-irradiated regions were analyzed by a scanning electron microscope (SEM, Hitachi 4300 SE) in a water vapor environment to eliminate charging effects. Local crystallinity and orientation were determined by electron backscatter diffraction (EBSD) with Kikuchi patterns collected by a Hikari detector within the SEM column. The EBSD pattern scans were collected and indexed using TSL OIM Data Collection software, whereas Orientation Imaging Microscopy Analysis software yielded crystal orientation deviation (COD), pole figure (PF) and inverse pole figure (IPF) maps[17]. The chemical compositions were determined at multiple locations on each sample by an energy dispersive detector attached to SEM, using EDAX-Genesis software.

The crystallinity and orientation of the laser created dots and lines were further examined by scanning Laue X-ray microdiffraction (μSXRD) with submicrometer spatial resolution on beamline 12.3.2 of the Advance Light Source synchrotron, Lawrence Berkeley National Laboratory[18]. Polychromatic x-ray beam with an energy range of 6-22 keV was focused to submicron size via a pair of elliptically bent x-ray mirrors in a Kirkpatrick-Baez configuration. Samples were raster scanned under the x-ray beam with a step size of 1 micron. At each step a Laue pattern was collected using a DECTRIS Pilatus 1 M hybrid pixel detector. Indexing of the Laue patterns was completed using the XMAS software[19].

RESULTS AND DISCUSSION

General considerations of RLS crystal architecture. As noted previously[11], the lattice of single crystal line formed on the surface of glass by laser-induced solid state glass → crystal

transformation undergoes gradual rotation to accommodate the density mismatch between the glass and crystal. The rate of this rotation ($\Theta = \theta\,°/\mu m$)) varies significantly with the orientation of crystal line relative to growth direction, as demonstrated in Figure 2. Here several independent crystal lines were written in different directions starting from the same central position D1 of the previously fabricated line marked L0 on the surface of $16SbI_3$-$84Sb_2S_3$ glass. The new crystals marked L1-L6, and L8 were formed as straight lines, whereas a bend was added to L6 at a later stage and form crystal line L7. It is particularly striking that for all these lines the axis of rotation is parallel to sample surface and normal to growth (scanning) direction. However, the magnitude of rotation rate varies depending on the direction of laser scanning. It may change to another value if a bend is created in the direction of crystal growth, as seen for the crystal line L6 turning into line L7. The crystal lattice rotates downward in all the lines as marked for each case in Figure 2c. The crystal orientation deviation (COD) map in Figure 2d describes the rotation of various RLS crystal lines quantitatively.

To obtain further insight of the space orientations of crystal lines, we have analyzed the pole figure map as seen in Figure 2e. We learn that the crystallographic direction [100] is practically normal to the surface of the sample and can be used for describing the variation of crystal orientation in space. As seen from magnified pole figure map (e) for [100] of Sb_2S_3 crystal, the rotation of the unit cell completely reproduces the topology of laser scanning of crystal lines. It confirms that the observed rotation of the crystal lattice strongly correlates with the spatial orientation of crystal growth direction that parallels the scanning direction of the laser beam.

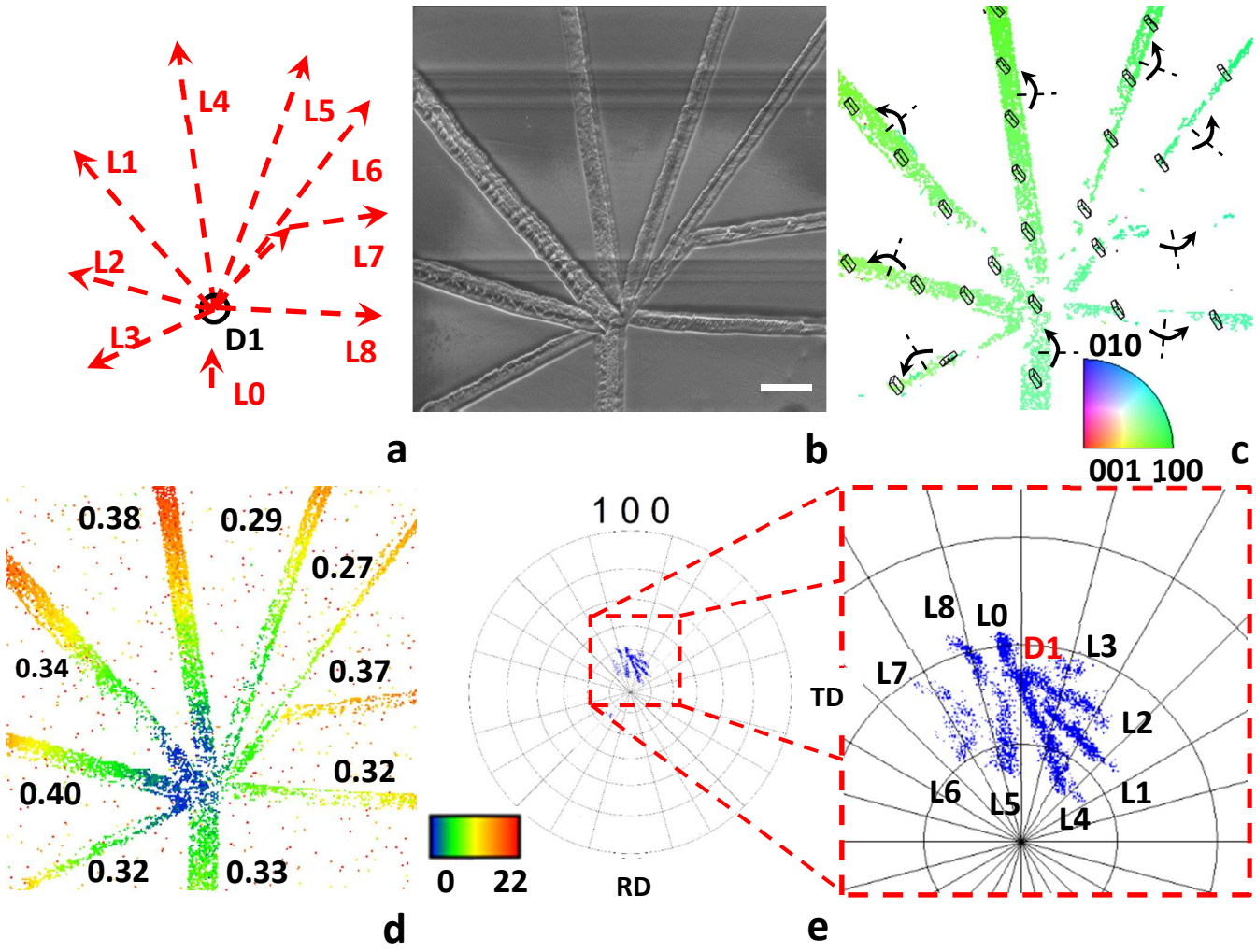

Figure 2. Rate of lattice rotation as a function of the direction of laser-induced crystal growth. The initial crystal dot seed was created by slowly ramping the power density from 0 to 90 mW/μm^2 in 5s, followed by steady exposure for 60 s. After forming the seed crystal line L0 was written by moving sample relative to the laser spot at 20 μm/s in nitrogen environment on the surface of $16SbI_3$–$84Sb_2S_3$ glass. The end (D1) of the created line L0 was used as seed for growing additional independent crystal lines (L1-L8) in different directions, where the steady exposure time was reduced to 1 s. Protocol schematic (a); SEM image (b); orientation IPF map with reference vectors along surface normal (c); COD map with reference to crystal orientation at the center of the initial dot (D1) (d) ; pole figure map and its enlarged version (e) for the

crystal architecture. Arrows on IPF map (c) describe the axis and direction of the lattice cell rotations. Numbers in (d) indicate average rotation rate (in degrees/μm) for writing the lines, and the labels on (e) indicate the points which correspond to the lines of the crystal architecture. Scale bar corresponds to 10 μm.

Having demonstrated the initial feasibility of creating single crystal lines with a bend (for example, line L7 in Figure 2) on the glass surface, we continued to explore the creation of 2D crystal pattern using 'rastering' protocol as described in the Experimental section. To develop the idea of rastering systematically, at first we made a simplified test of the rastering process without joining successive lines, as shown in Figure 3. Here the crystal architecture was fabricated from an initially nucleated dot D1 at the end of a previously formed single crystal line and the laser was moved relative to glass sample without interruption or alteration of laser beam irradiation conditions. The specific pattern was created by moving the laser spot at the speed of 20 μm/s. At the end of a given line (vertical segment V1-V7 in Figure 3), the laser was turned by 90° creating an orthogonal segment or pitch of 7 μm (horizontal segment H1-H7) by scanning in *y*-direction. Figure 3 shows SEM image and EBSD maps of such a crystal pattern. The pitch of 7 μm is approximately two times larger than the width of the crystal line (~4 μm). In this case all segments – horizontal or vertical on the figure – were surrounded by the glass phase; thus any overlap or interaction between the segments was avoided. Figure 3c shows the variation of lattice orientation within this single crystal architecture, including the varying orientation of the crystal's unit cell and IPF map for normal direction i.e. ND map. Clearly, the lattice of RLS crystal rotates in both the horizontal and vertical segments about an axis, which is parallel to the sample surface and normal to the length of the corresponding segment. For vertical segments the

rotation axis is horizontal, and for horizontal lines, conversely, the rotation axis is vertical; all axes remain parallel to the sample surface.

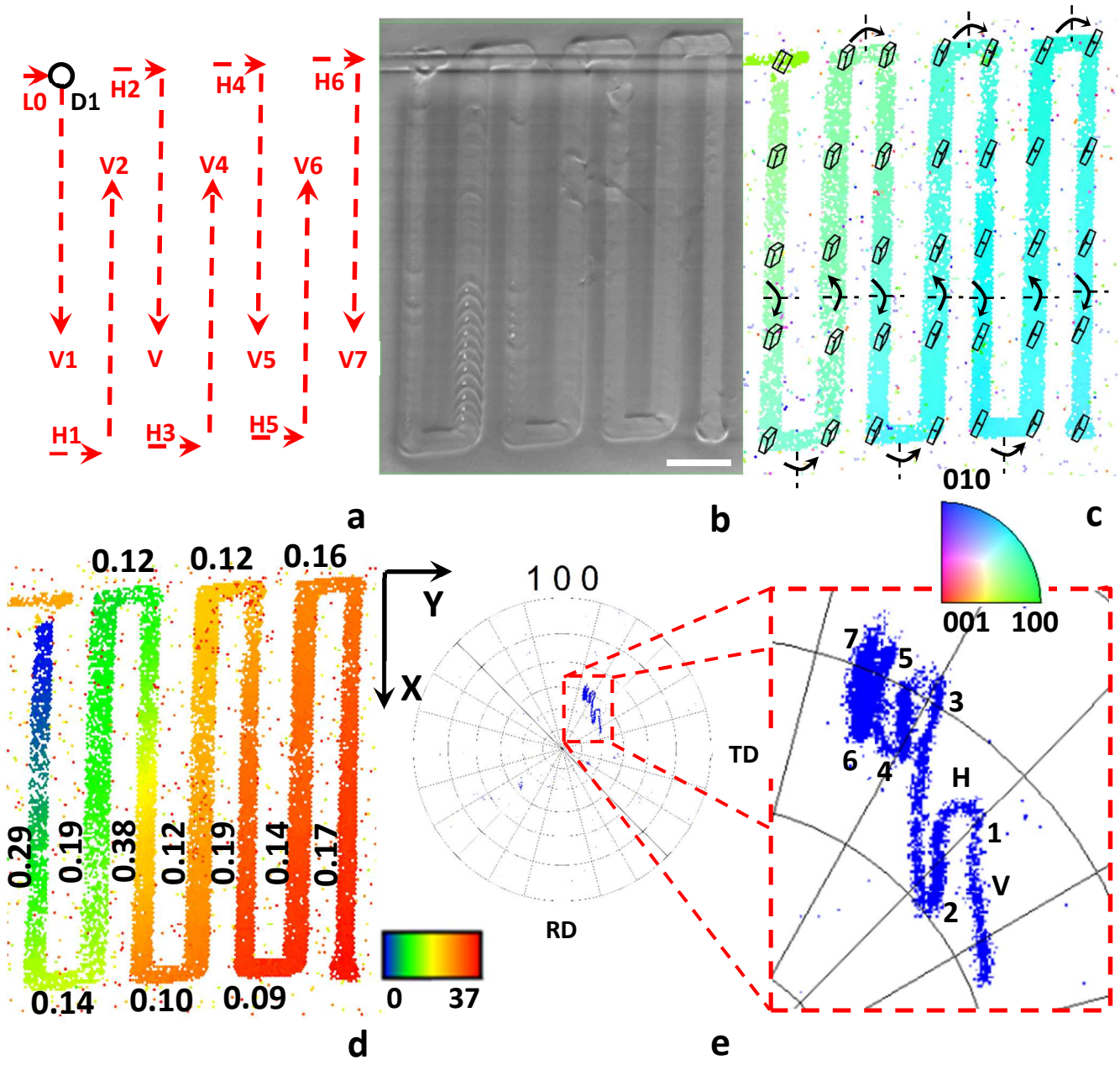

Figure 3. The 2D single crystal pattern created using rastering protocol with 7 μm step on the surface of $16SbI_3$-$84Sb_2S_3$ glass. The previously laser-induced line was used as seed for growth. Pattern was created as a raster by moving the laser spot with scanning speed 20 μm/s in nitrogen environment. Scale bar corresponds to 10 μm. Plan-view (a) and SEM image (b), orientation IPF

map with reference vectors along surface normal (c), crystal orientation deviation map relative to the crystal orientation at beginning of the initial line (V1) (d), pole figure map and its enlarged version of the crystal architecture (e). The arrows in (a) indicate the direction of laser motion relative to sample and arrows on IPF map (c) describe the axis and direction of the lattice cell rotations. Numbers in (d) indicate average rotation rate (in degrees/μm) for writing the lines, and the labels on (e) indicate the points which correspond to the lines of the crystal architecture.

Further details of the spatial orientation of local lattice of the vertical and horizontal RLS crystal line segments are obtained from pole figure map. As for previous 1D crystal architectures the crystallographic direction [100] is practically normal to the surface of the sample and therefore well suited for presenting the variation of crystal orientation in space. This magnified pole figure map for [100] in Figure 3e clearly distinguishes lattice rotation in vertical and horizontal segments, which represent crystal lines of a potential 2D pattern to be created by the rastering protocol. On this pole figure map their lengths are proportional to the corresponding rotation rate and the length of crystal line. For example, vertical lines V1 and V3 show relatively high value of rotation rate, 0.29 and 0.38^{o}/μm – see Figure 3d, respectively. The corresponding segments are the longest on the pole figure map in Figure 3e. By contrast, the rotation of horizontal crystal lines H5 and H6 is close to zero. Consequently, the three vertical segments, V5-V7 practically overlap. Once again the lattice rotation of crystal lines completely reproduces the direction of laser scanning during rastering. These results confirm what we discovered previously for 1D lines: the direction of rotation depends on the laser scanning direction relative to the initial seed. Note that in Figure 3 as the laser beam makes U-turn, the lattice rotation also makes U-turn; the trajectory of rotation completely reproduces the trajectory of laser beam, which can be readily seen in the pole figure map in Figure 3e.

There are some directions for which there appears to be no rotation of lattice within the experimental uncertainty[11]. Such a Sb_2S_3 crystal line was written in the crystal's (010) plane along <001>. This orientation of crystal belongs to its primary slip system (010)/[001], experimentally established for free-standing, natural Sb_2S_3 crystals[20], which is, as expected, also the direction of shortest bonds (i.e. most dense packing) on the closest packed planes for its crystal structure[21,22]. The results obtained from the experiments described above guide the fabrication of macroscopic 2D crystals: *To minimize lattice rotation within an RLS crystal we should use crystal seed with (010) plane parallel to glass surface and perform laser scanning in <001> direction.*

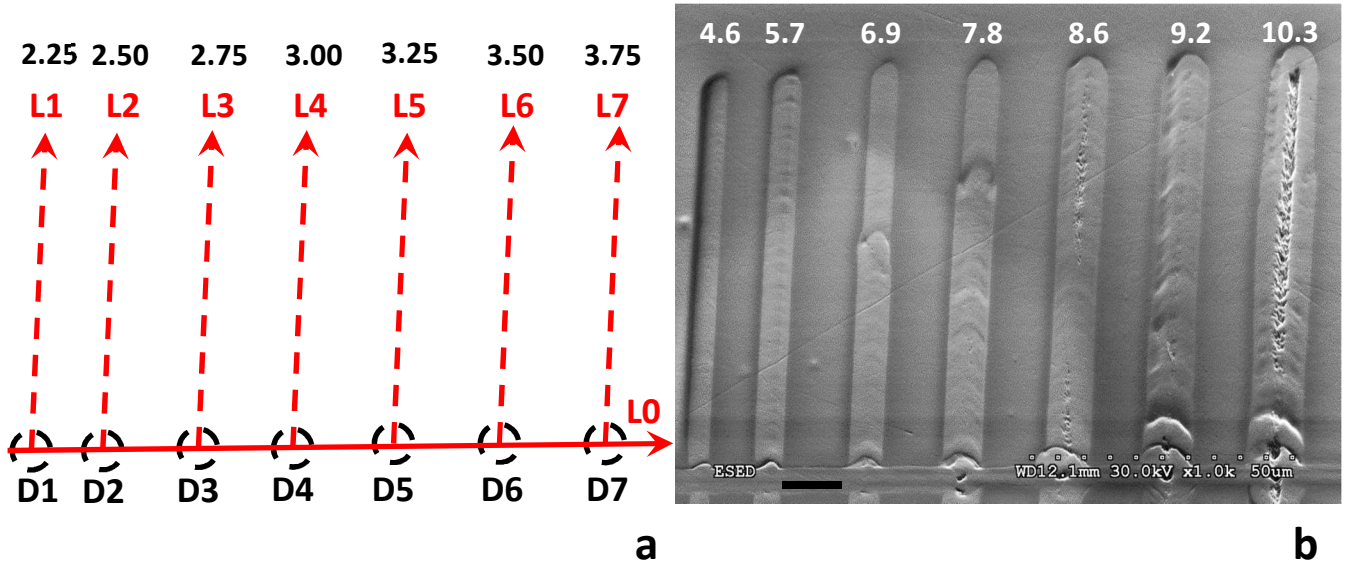

Figure 4. Effect of laser power on the formation of single crystal lines. The initial crystal dot was created by slowly ramping the power density from 0 to 90 mW/μm^2 in 5s, followed by steady exposure for 60 s. Thereafter, the seed crystal was grown to form crystal line L0 by moving the laser spot linearly at 20 μm/s on the surface of $16SbI_3$–$84Sb_2S_3$ glass. Next, line L0 was used as seed for growing seven crystal lines L1-L7 with different laser power, starting at dots D1-D7, respectively. The steady exposure for forming each dot before growing the lines

was reduced to 1 s. Scheme for forming the lines (a), where the arrows indicate the direction of laser motion relative to sample; SEM image of the crystal architecture (b). Numbers at the top in (a) indicate laser power (in mW) for writing the lines, and the numbers on (b) indicate the width of the lines in micrometers. Scale bar corresponds to 10 μm.

An improvement that we may attempt for fabricating large 2D single crystal is to widen each crystal line as much as possible. It can be implemented by increasing the laser power and/or beam size. Even though the width of the crystal line is increased, increasing the laser power is problematic because the intensity in the center becomes too high such that evaporation occurs in the center here[16] - see Figure 4. In order to avoid this complication, we defocused the laser beam by moving the objective up by about 5μm while increasing the laser power. To study the influence of this approach we performed the following sequence of experiments (see Figure 5). First, a single crystal line, L0, is created, as before, to serve as the seed. Then, narrow single crystal lines L1-L3 are grown as before, using the beam that is focused at the surface. Finally, these lines are used as seeds (D4-D6) for widening the narrow lines of Stage II to obtain significantly wider crystal lines, L4-L6, using defocused laser beam with different power densities. Using this approach and starting at D6, we obtained 18 μm wide single crystal line of Sb_2S_3 at 6 mW laser power without any evaporation in the center - see Figure 5. However, for the case of dots D5 and D6 that were produced using higher laser powers, evaporation was observed in the center of laser spot. In principle, this can be mitigated or eliminated by a shorter time of laser exposure or lower laser power in these regions.

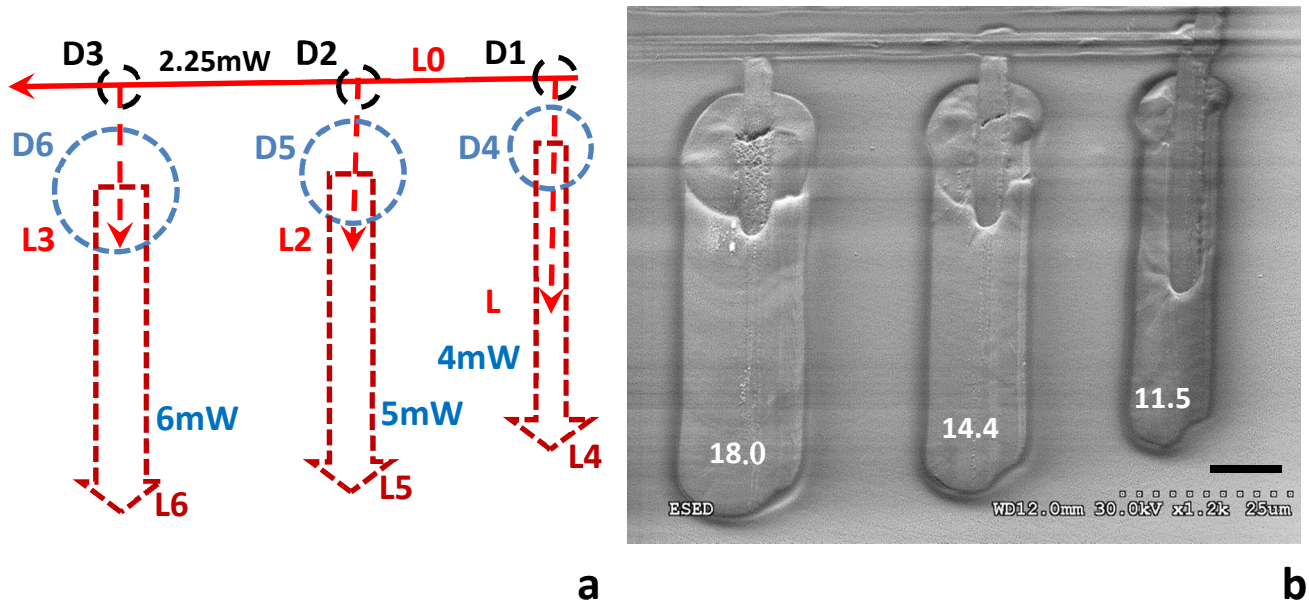

Figure 5. Laser-induced growth of wide single crystal lines on the surface of $16SbI_3$–$84Sb_2S_3$ glass**.** First a single crystal line L0 is fabricated as in Figure 2, providing correlated seeds D1-D3. Next, single crystal lines L1-L3, are grown as before (Figure 2). Finally, the newly formed lines L1-L3 are used as seeds (D4-D6) for growing broader crystal lines L4-L6, with the laser focused 5 μm above the surface and different powers (4-6 mW), as indicated in (a). Steady time exposure was reduced to 1 s. Scheme of fabrication process (a); SEM image of the crystal architecture (b). Numbers on (a) indicate laser power used for writing the lines, and the numbers on (b) show the width of lines in micrometers. Scale bar corresponds to 10 μm.

Fabrication of 2D Sb_2S_3 single crystal by "stitching" of 1D lines. Figure 6 shows prospects of 2D crystal growth of Sb_2S_3 on the surface of $16SbI_3$-$84Sb_2S_3$ glass using stitching protocol. A key issue in this case, is to establish under what conditions a new crystal can be nucleated in the vicinity of a previously formed crystal line so that the two join without a seam. With this in mind, at first, a crystal seed dot (D1) was formed on the surface of glass by slowly ramping the

power density from 0 to 90 μW/μm^2 in 5s followed by a steady laser exposure for 60 s (see Figure 6a).

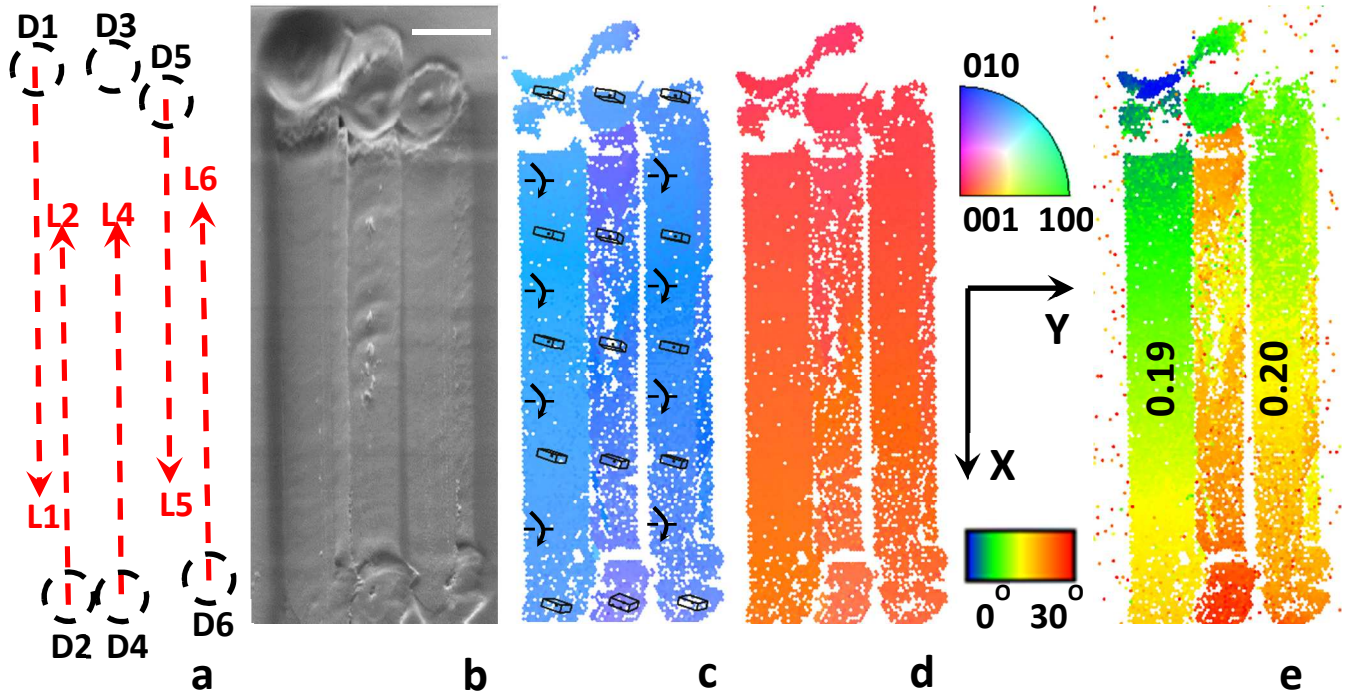

Figure 6. Demonstration of 2D laser-induced crystal architecture using the 'stitching' of five Sb_2S_3 single crystal lines on the surface of $16SbI_3$-$84Sb_2S_3$ glass. Scale bar corresponds to 10 μm. Schematic of stitching protocol, where the arrows indicate the direction of laser motion relative to sample (a); SEM image (b); inverse pole figure (IPF) maps of the region with reference vectors along surface normal (c) and in-plane x-direction (the rolling direction, RD) (d) of the 2D crystal architecture; and corresponding crystal orientation deviation map from the crystal orientation in the initial dot (D1) (e). The arrows on IPF map (c) describe the axis and direction of the lattice cell rotations. Numbers in (e) indicate average rotation rate (in degrees/μm) for writing lines of the crystal architecture.

The crystal nucleation rate for $16SbI_3$-$84Sb_2S_3$ glass composition is slow, taking 40-50 seconds before the appearance of a seed crystal upon heating with laser as described above for the initial

dots in Figure 3 or 5. When the sample is moved at the speed of 20 μm/s in *x*-direction, the crystal grows without introducing additional nuclei. Thus the first 1D single crystal line (L1) of length 100 μm was obtained. To obtain the next crystal line, the sample was shifted in *y*-direction by a few microns from the position at the end of previous line L1 to position D2. Next, the first line was used as the seed and the second line was written parallel to the first line in reverse direction. Scan #3, which started from D3 position was performed without the laser beam and line L4 was created from D4 position, which had the same *y*-coordinate as D3. The above mentioned procedure of line writing was repeated two times more (L5 and L6) using the same experimental conditions. The steady time exposure for forming dots D2 and D4-D6 was 15 s.

The process of 'stitching' of individual lines was tested with different values of inter-line spacing, *s,* when starting the new line. The EBSD analysis shows that neighboring lines stitch almost 'seamlessly' when *s* is sufficiently small, for example, 3 μm for lines L2 and L6 in Figure 6; EBSD maps indicate that there is no grain boundary between them in Figure 6b-6e. The neighboring lines appear to merge and form one wider single crystal. For large *s* (6 μm), however, EBSD analysis indicates the presence of a high angle boundary between L2 and L4 lines, or a layer of amorphous solid between L4 and L5 lines. In inverse pole figure maps (c) and (d), the colors represent the orientation of crystallographic axes of Sb_2S_3 crystal, as described in the legend. Figure 6e shows a COD map with respect to crystal orientation of the center of seed dot D1, amplifying lattice orientation variations. The red color of IPF map for rolling direction (RD), which corresponds to the laser scanning direction, demonstrates that crystals of Sb_2S_3 phase grow in the same direction that is close to <001> crystallographic direction in all lines in Figure 6d. By comparison, the IPF map for the normal direction (ND) shows clearly abrupt changes in color between L2, L4 and L5 lines in Figure 6c. Color change of lines in the ND map

indicates that the orientations of the crystal lines in direction normal to the surface of sample are different. Crystal orientation in ND analysis varies up to 12° for the crystals of L2 and L4 lines and between L4 and L5 lines - see, for example, Figure 6e. That is, there appears to be a difference between the orientations of the neighboring crystal lines, which depends on the magnitude of *s*. It is shown clearly in Figure 6e that the orientation of crystal lattice of line L4 (or L5) with large *s* follows the orientation of the initial dot D4 (or D5), and not the orientation of previously created neighboring lines L2 (or L4).

Additionally, as it was reported recently for RLS crystal lines[11], there is a subtle gradual variation of color in Figures 6c and 6d along *x*-direction for each line. This gradual change in the orientation of crystal lattice that occurs for all the lines when viewed along the ND and RD directions is further elucidated by the COD map in Figure 6e. A comparison of these maps and space orientations of unit cells shown for a few selected points on the lines in Figure 6c indicates that the <010> and <001> orientations of the crystals rotate around the *y* in-plane direction, which is normal to the laser scanning direction (i.e. the *x* or RD). The average rate of lattice rotation ($\Theta = \theta°/\mu m$) was found to be 0.19±0.02°/μm for L1 and L2 and 0.20±0.02°/μm for L5 and L6 lines. Also from space orientations of the unit cell the sign of the rotation depicted in Figure 6c was obtained. The results show that the crystal lattice rotates downward in Figure 6c as one traverses along the lines, confirming what was observed for RLS crystals in the previous work[11].

Figures 7 and 8 show more detailed examples of 2D single crystals also fabricated following stitching protocol. They describe the results of EBSD mapping for two laser-written single crystal regions, in which the laser spot was shifted in *y*-direction either with *s* = 4 μm (Figure 7) or 3 μm (Figure 8) between successive lines. The laser power, scanning speed, and time of

exposure were kept the same for both examples. Symbol D1 indicates the initial laser focal point. The width of one isolated line (for example, L4 in Figure 6)) was ~7 μm, so a step with s = 3 μm represents overlap between successive lines. On the other hand, a step with s = 4 μm would produce a new line crystallizing from glass without the knowledge of the previously formed line. The results in Figures 7 and 8 show that for the former case with s = 3 μm, the lattice orientation of the laser-written region does not exhibit any sudden change of crystal orientation within the region, representing a 2D single crystal. By comparison, the 2D pattern formed with s = 4 μm consists of single crystal lines that have different crystal lattice orientations (see Figure 7). A comparison of these two scenarios suggests that two successive lines are stitched together seamlessly, forming a 2D single crystal region if the step in y-direction is less than half the width of an independent single crystal line fabricated using the same laser writing conditions. This observation would appear reasonable considering that the hottest point of the Guassian shaped laser beam is at its center from where the crystal begins to grow. It is remarkable, however, that the new line takes the orientation of the previously formed line. It means that the adjoining region of the previously formed line serves as the seed and no new independent nucleation is needed. Consequently, much less time is needed to start the growth process as compared to the formation of the very first seed, D1. This mechanism of seamless stitching of two successive lines is totally consistent with the all solid state glass → crystal transformation that ensues during the heating of glass rather than the cooling of melt.

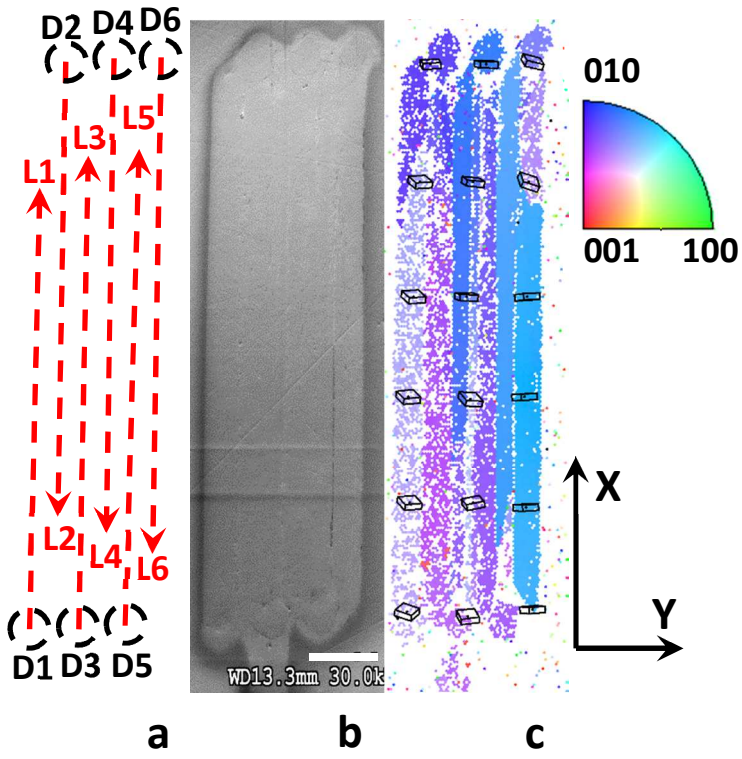

Figure 7. 2D laser-induced crystal architectures stitching a few lines created with constant 4 μm step shifting. The laser scanned 2D regions after repolishing. Scale bar corresponds to 10 μm. Schematic of writing protocol (a); SEM images (b), and colored orientation IPF maps of the 2D crystal architectures with the reference vector along surface normal (c). The arrows in (a) indicate the direction of laser motion relative to sample.

The EBSD maps indicate that the 2D laser-crystallized pattern starting from a single dot D1 is essentially a single crystal (Figure 8), as there is no abrupt change of orientation to indicate the presence of grain boundary. However, a more careful analysis reveals a gradual, but continuous rotation of the lattice about *x*- and *y*-directions parallel to sample surface - note the smooth and gradual changing of color of EBSD map in Figure 8c, which occurs along both the scanning (*x*) and step shifting (*y*) directions of this crystal architecture. Figure 8d shows this variation more clearly on the COD map, where lattice orientation changes are amplified, with reference to the

lattice orientation at the center of seed dot D1. This COD map clearly shows a gradual rotation of crystal lattice for each line of the architecture. The orientation of the unit cell of Sb_2S_3 crystal lattice changes gradually as marked schematically on the first crystal line of Figure 8c. Here, as one moves along the scan direction, the lattice rotates downwards about the axis that is in the plane of crystal, which is also the sample surface, and normal to the direction of laser scanning. Similar to one isolated crystal line, the 2D pattern also shows gradual rotation for all lines around the axis normal to crystal growth direction (in this case *y*-direction). But, in contrast to the isolated line, the unit cell of the 2D Sb_2S_3 crystal gradually rotates around another direction of the architecture, namely *x*-direction, which is parallel to scanning direction (see Figure 8c). To explain this additional rotation, we need to take into account that upon shifting in regions D2-D7 the crystal grows in *y*-direction, so there the lattice rotates around *x*-direction. During the subsequent creation of each new line by laser displacement along *x*- direction, the crystal growth is guided by a combined influence of the newly formed dot and the local orientation of the preceding line. It starts with the orientation of the respective seed dots and then rotates around *y*-direction during the line scan. On the magnified pole figure map in Figure 8e for crystallographic direction [110], which is close to the normal to sample surface, we cannot distinguish separate lines of the pattern. A rectangular profile of PF space distribution for [110] indicates that the unit cell of the Sb_2S_3 crystal rotates around a direction that has components along both the orthogonal *x*- and *y*-directions of the 2D architecture.

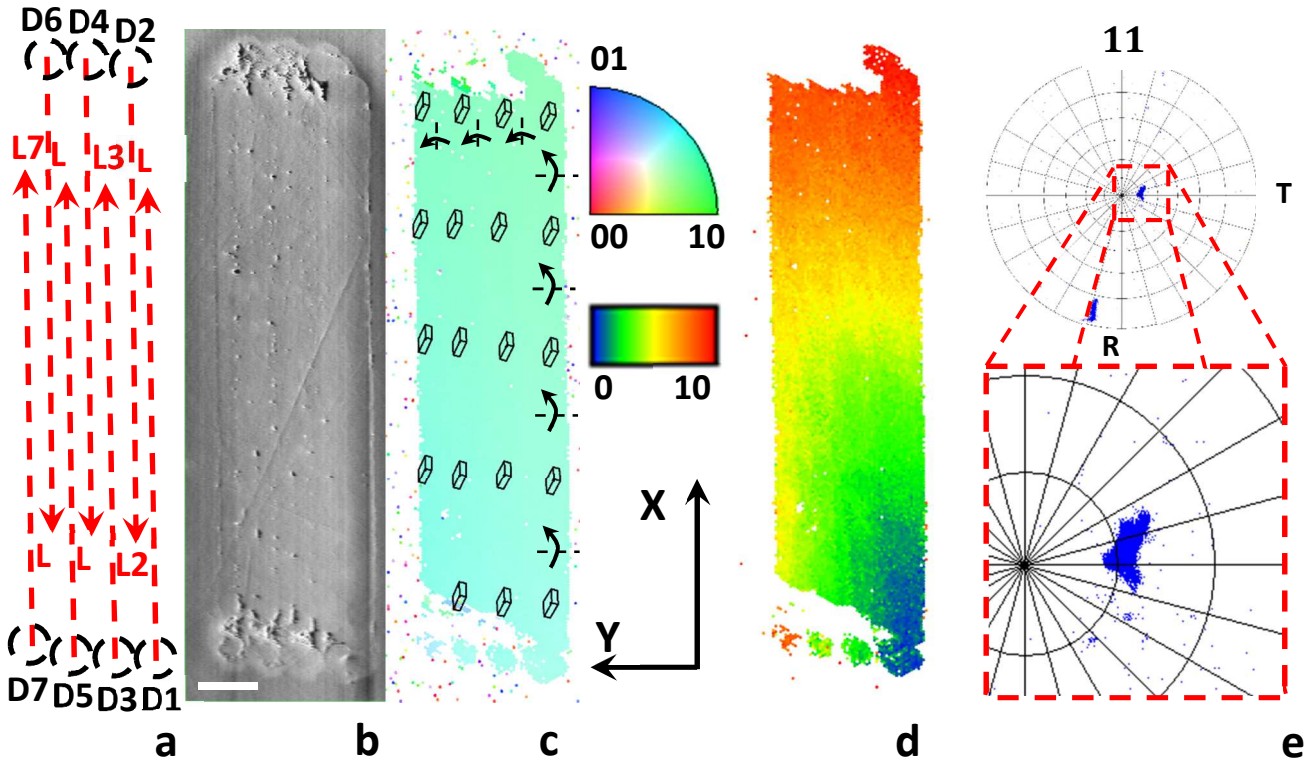

Figure 8. 2D laser-induced crystal architectures stitching a few lines created with constant 3 μm step shifting. The laser scanned 2D regions after repolishing. Scale bar corresponds to 10 μm. Schematic of writing protocol (a); SEM images (b), colored orientation IPF maps of the 2D crystal architectures with the reference vector along surface normal (c) and corresponding crystal orientation deviation map relative to the crystal orientation at the center of the initial dot (D1) (d); pole figure map for [110] crystallographic direction and its enlarged version obtained by EBSD (e). The arrows in (a) indicate the direction of laser motion relative to sample.

Fabrication of 2D single crystal by continuous rastering of 1D line. To apply the knowledge gained from the experiments described in Figures 2-5 to fabricate 2D structure following the rastering protocol, line L0 (similar to line L4 in Figure 5) was formed by the laser beam focused 5 μm above the surface with 4 mW power intensity as shown in Figure 9. The so created wide line L0 with width 11-12 μm was used as a seed (D1) for fabricating 2D single

crystal using the rastering protocol with 10 μm pitch and no change in the laser beam conditions. A successful example of this methodology is shown in Figure 9, where each line was 50 μm long (*x*-direction in the figure) and the next line was shifted by 10 μm from the preceding line in the *y*-direction. Since the width of each line was 11-12 μm, the selected spacing provided an overlap of every forthcoming line with previously induced line by 1-2 μm. The COD map of the 2D pattern in Figure 9d shows gradual but small color change only between the lines in *y*-direction ($<0.1^0/\mu m$); there is virtually no rotation along the lines (*x*-direction in the figure). The EBSD results indicate that the present lines grow in <001> crystallographic direction with {010} plane parallel to glass surface. Evidently, for this direction the density of dislocations, which compensate mismatch and cause rotation of lattice cell, is lower than for the [100] crystallographic direction that is parallel to the *y*-direction of rastering. On the magnified pole figure map in Figure 9e for crystallographic direction [010], which is close to the normal to sample surface, we cannot distinguish separate lines of rastering. Instead, we find a rectangular profile of space distribution for [010], which indicates that the rate of rotation in *x*-direction (laser traversing along crystallographic [001]) is lower than in *y*-direction (along crystallographic [100]).

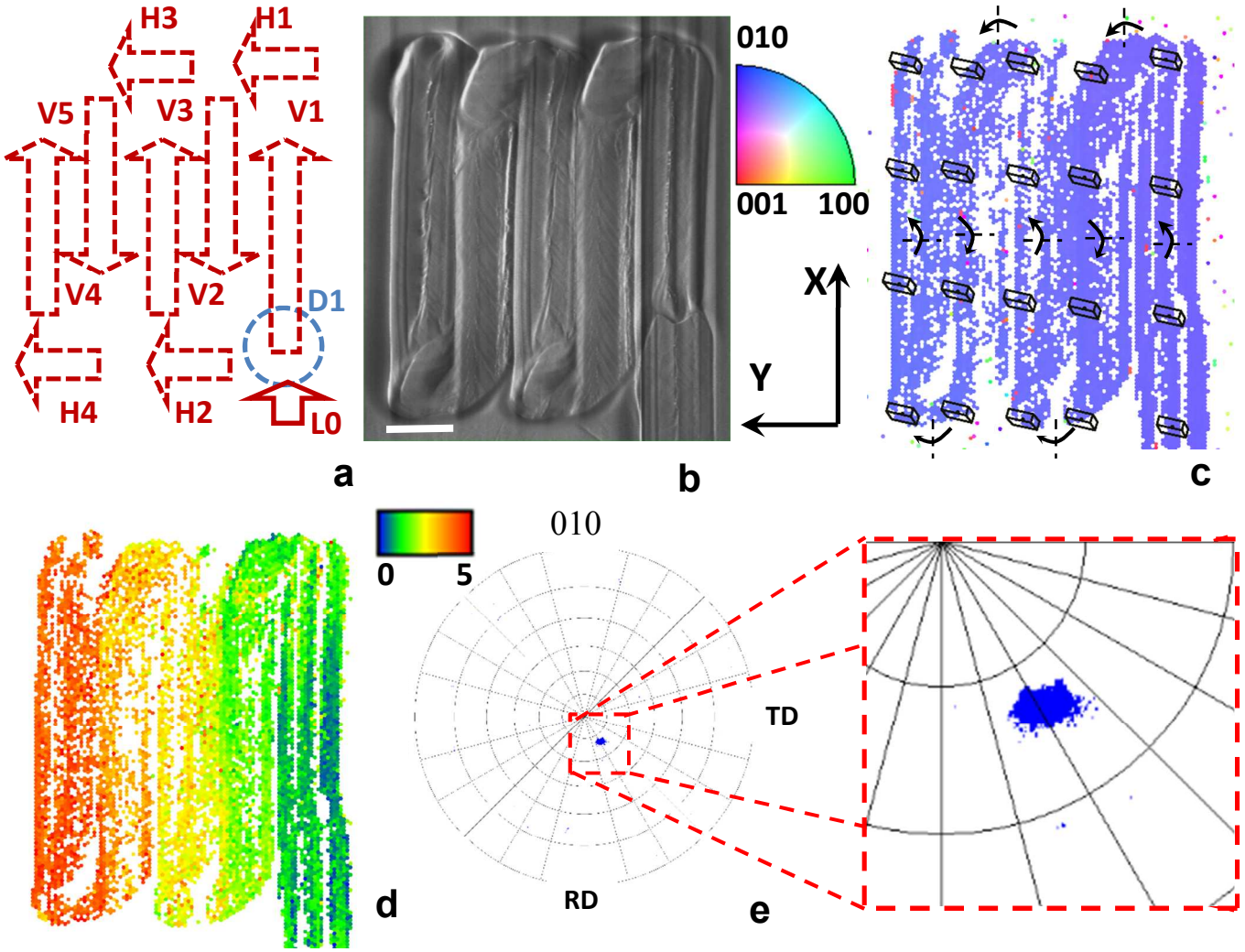

Figure 9. The 2D single crystal pattern created on the surface of $16SbI_3$-$84Sb_2S_3$ glass using modified rastering protocol. Here a previously laser-written single crystal line was used as seed for growth. The 2D single crystal pattern was formed with the laser focused at 5 µm above the surface and the intensity of laser beam was 4 mW. The pattern was created by rastering with 10 µm pitch and a scanning speed of 20 µm/s. Scheme of fabrication process (a); SEM image (b); orientation IPF map with reference vectors along surface normal (c); COD map with reference to the crystal orientation of the initial dot (D1) (d); pole figure map and its enlarged version of the crystal architecture (e). Arrows on IPF map (c) describe the expected axis and direction of the lattice cell rotations. Scale bar is 10 µm.

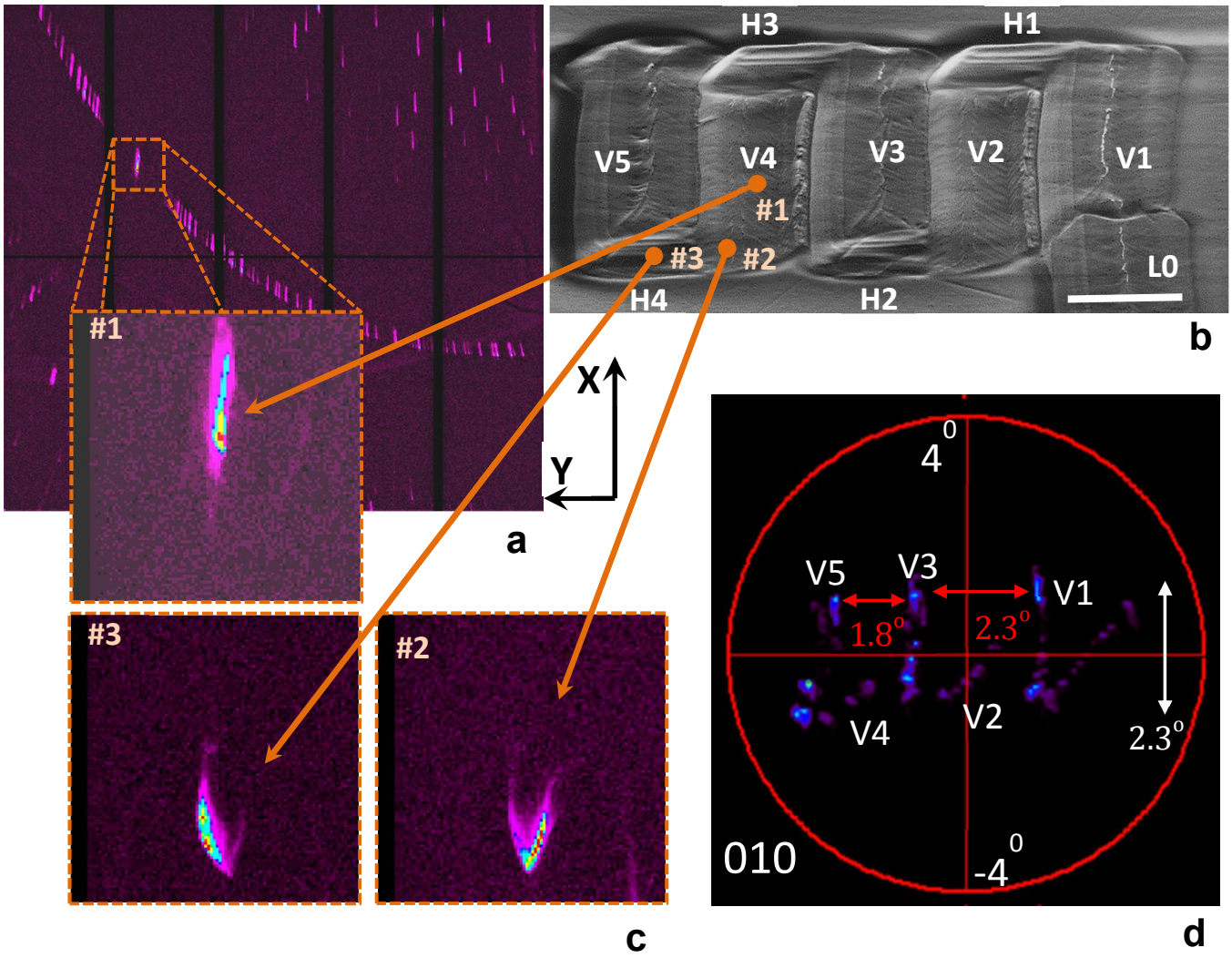

Figure 10. Results of μSXRD of 2D Sb_2S_3 crystal architecture shown on Figure 9. Full Laue diffraction image (a); SEM image (b) of the 2D crystal with specific points that we analyzed; magnified images (c) of (020) reflection as extracted from the Laue pattern in (a) for three different points of the crystal marked in (b); magnified pole figure map for [010] crystallographic direction of the crystal architecture (d). The labels on (d) indicate the points which correspond to the lines of the crystal architecture.

To complement the lattice orientation information provided by EBSD that has excellent spatial resolution but very shallow probed depth (a few nm) and relatively poor diffraction angle

accuracy (typically, 1-2°), we examined the same 2D pattern of Figure 9 with μSXRD that has much higher orientational accuracy (typically, ±0.01°), a micron size spatial resolution and probe depths up to ~100 μm. The evolution of lattice orientation as manifested in Laue spots is shown in Figure 10 for this 2D crystal. As an illustration, Laue spot corresponding to (020) crystallographic planes is analyzed in detail. The diffraction from the scanned line of 2D laser-written crystal, for instance, point #1 on Figure 10a shows a Laue spot that is steadily elongated with a rod-like intensity distribution (Figure 10c). Similar μSXRD Laue magnified images comprising of uniaxially elongated streaks were observed previously for 1D RLS crystal lines[11]. Such streaks were interpreted as representing unpaired randomly distributed dislocations and their ordered assemblies like small angle grain boundaries, disclinations, etc., in the crystal. The relative shift of the same Laue reflection for three locations #1, #2 and #3 within the same line (see magnified images of the three points in Figure 10c) indicates the presence of lattice rotation. It is shown systematically by the pole figure map for [010] crystallographic direction in Figure 10d from Laue data, as well as by the EBSD map in Figure 9. The much higher resolution of the pole figure configuration by μSXRD than EBSD is very clear from a comparison of these two figures.

As soon as the laser makes a 90^{o} bend to form a new line (points #2 and #3 in Figure 10b), the diffraction from this region shows a similar bend of the shape of reflection and diffuse scattering around the reflection spot in Figure 10c. The pole figure map in Figure 10d for a part of 2D pattern comprises three vertical segments identified as V1, V3 and V5, along with two slanted vertical interconnections identified as V2 and V4, respectively. This map appears similar to the pole figure map observed from EBSD for the 2D raster shown in Figure 3e. The difference between these patterns is quantitative and qualitative. The first laser-scanned pattern formed with

a pitch of 7 μm in Figure 3 indicates lattice rotation of up to 37°, then the total misorientation for the second pattern is less than 5° (Figure 9). Note that the vertical segments of the first four lines V1-V4 of the pattern in Figure 3e have different lengths; here the crystal lines exhibit different average rotation rate in +*x* and -*x* scanning directions, Θ: 0.29 and 0.38°/μm for V1 and V3 and approximately two times smaller values of 0.19 and 0.12°/μm for V2 and V4 sections. In contrast, for the pattern with overlapping lines in Figure 10d, the length of vertical segments V1, V3 and V5 are the same with θ_x=2.3° for 50 μm long crystal lines. It means that the *x*-components of rotation along these lines are the same. Further, the distance between these vertical segments indicates the *y*-component of rotation, θ_y. They are parallel to each other in Figure 10d, which means constant *y*-component of rotation between these lines over their whole length.

The behavior of segments for V2 and V4 crystal lines is fundamentally different than that of the vertical lines V1, V3 and V5. Most obviously, the corresponding segments of PF map are not vertical but change gradually, in contrast to those of V1, V3 and V5 lines. So the V2 and V4 lines simultaneously show rotation along *x*- and *y*-directions - vertical and horizontal directions on the PF map in Figure 10d, respectively. Evidently these lines grow with a rotation of lattice around an intermediate direction that is between *x*- and *y*-directions. The *x*-rotation is still the same as for the odd lines, but in addition there is also an additional *y*-component of rotation even though the laser is scanned in -*x* direction! Apparently, in these cases the crystal grows not in exactly -*x*-direction but at an angle relative to the -*x*-scanning direction, which introduces a *y*-component to the overall rotation. This observation is somewhat unexpected considering relatively small overlapping of 1-2 microns between the lines. A rotation with *y*-component implies deviation of crystal growth of line from *x*-scanning direction. The magnitude of this

component is expected to increase as the overlap with the preceding line increases, for example, in the pattern created in Figure 8 by the 'stitching' protocol. The difference in the PF maps of odd and even numbered lined in Figure 10d suggests that there are additional factors that determine the *y*-component of rotation within a line.

Comparison of 2D single crystals formed by stitching and rastering protocols. It is interesting to compare the lattice rotation that occurs in the 2D single crystals prepared by the two methods of fabrication, viz. stitching vs. rastering. In this regard, note that lattice rotation indicates how the amorphous structure of glass transforms into a periodic lattice of the appropriate single crystal in the presence of stresses from density change, which vary dynamically as the laser moves and the structure of the surrounding glass and crystal relaxes[11]. In the creation of 1D straight lines, this type of crystal growth within the confinement of a glass matrix introduces randomly distributed unpaired dislocations and small angle grain boundaries made of organized dislocations. The net result is a smooth rotation of the lattice along the direction of laser scanning, as seen in Figure 2 for various straight lines. However, the situation becomes complicated when fabricating 2D crystals. As seen in Figures 8 vs. 9 and 10, there are both similarities and differences between the rotations in the two cases, when the lines of 2D architectures are prepared by stitching vs. rastering protocols. In general, both processes produce lattice rotation in both the *x*- and *y*-directions. Also, the fundamental mechanisms of crystal and lattice rotation remain unchanged: at the end of the first and subsequent lines formed by scanning along *x*-direction, the new line begins with growth along *y*-direction as the laser beam is moved along *y*-direction. In this segment, the lattice rotates around *x*-direction. Thereafter, as the laser direction is turned to move along *x*-direction, the rotation is determined by a combined effect of the orientations of the preceding line and newly formed *y*-segment. The extent of overlap

between the preceding and newly forming lines, which could be different for the two protocols, is a more explicit parameter that determines the relative values of the *y* component of overall rotation of the 2D pattern.

In the case of stitching, a new dot overlapping with the previous line is formed. The orientation of this "half dot" is controlled by the orientation at the end of the first line since it mainly grows in *y*-direction and the lattice rotation follows this growth direction: the crystal lattice rotates according to the *y*-component of misorientation relative to the end orientation of the previous line. Then from this newly formed dot, as the second line is grown overlapping with the previous line, the orientation of the lattice can follow two different scenarios, which depends on the orientation of growth direction relative to lattice orientation. On one hand, crystal may grow in *x*-direction from newly formed dot, independent of the previous line. On the other hand, the new line can form from the preceding line via growth along some direction, which is at an angle to the laser scanning *x*-direction. In both cases the new lines of 2D structure incorporate rotation in *x*-direction, but under the second scenario the crystal lattice incorporates an additional *y*-component of rotation. For example, this was observed for the even numbered vertical lines (V2 and V4) of the rastering pattern shown in Figures 9 and 10.

As the extent of overlap between successive lines increases, we may expect higher chances for realizing the second growth scenario. In this context it is instructive to inspect the rotation of crystal orientation in the 2D pattern shown on Figure 8. We examined this pattern using μSXRD that has much higher orientational accuracy than EBSD. The resulting behavior of the 2D crystal's orientation is seen as its pole figure map in Figure 11 for [110] crystallographic direction, which is close to surface normal. In this 'stitching' pattern four odd numbered vertical segments (L1, L3, L5 and L7), which correspond to four crystal lines of the pattern written by

laser translation along +*x*-direction are analyzed. We note that the intensity of Laue reflections for the three even numbered lines written in –*x* direction is too low to be observed on PFM. A plausible explanation for this difference in the two types of lines is as follows: The energy band gap for the glass matrix and Sb_2S_3 crystal is different: 2.0 eV and 1.5 eV, respectively. We employed 640 nm (=1.94 eV) laser, which is a little below the bandgap of glass and significantly larger than that of the crystal. Consequently, absorption and penetration depth of the laser beam should be different for the two regions. For these reasons, the first crystal line would have the largest thickness. The second line, which is made by overlapping the laser both the preceding crystal line and glass regions would be thinner, because half of the beam would illuminate preceding line and temperature distribution will be different than in the case of the first line. The third line would again have a different temperature distribution then the second line with smaller thickness than the first line, as shown schematically in Figure 12. Consequently, we observe periodic fluctuation in the intensity of X-ray diffraction from crystal lines seen in Figure 11. We do not observe this fluctuation of intensity in the EBSD pattern, because of the much smaller depth probed by electrons; only the high penetration depth of X-ray beam allows the differentiation of thickness via high and low intensities of Laue reflections from odd and even numbered lines. Other plausible reasons for this periodic variation of diffracted intensity are: unequal growth rates in +*x* and –*x* directions for polar Sb_2S_3 crystal[12], and different translations of the movement of sample stage. Further experiments are needed to unequivocally establish the origin of this interesting observation.

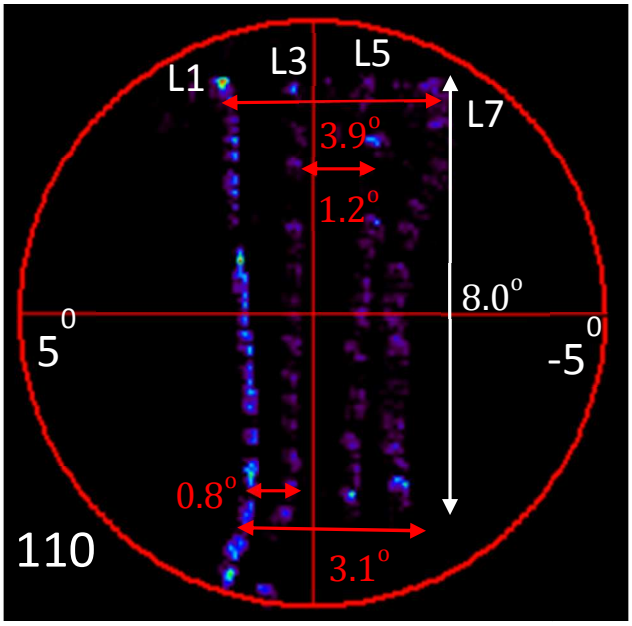

Figure 11. Magnified pole figure map of 2D Sb_2S_3 crystal architecture for [110] crystallographic direction as obtained from μSXRD of the crystal architecture in Figure 8. The labels indicate the points, which correspond to the lines in Figure 8.

We evaluate the orientation only of the odd numbered lines, viz. L1, L3, L5 and L7, which were written along +*x* direction, due to the readily detected intensity of their Laue patterns. Accordingly, the rotations of these four lines in *x*-direction have the same value of 8°. However, the gap between the segments varies from 0.8° to 1.2°, which represents the *y*-component of rotation between odd numbered lines. The other three even-numbered lines are located between these four odd-numbered lines, so we may expect very similar rotation for them too. Overall, for the 'stitching' pattern fabricated with an overlap of ~3-4 μm, evidently the crystal growth follows second scenario, wherein the crystal lines grow from the preceding line via growth at an angle relative to the laser scanning along *x*-direction. As a result, for different regions of the 2D pattern the rotation in *y*-direction varies from 0.8° to 1.2°.

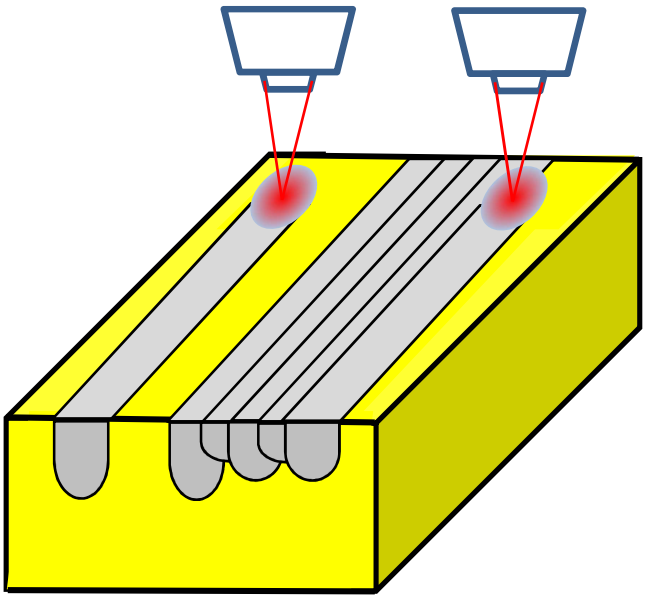

Figure 12. Different stages of 2D RLS crystal fabrication (first and fifth line of a pattern). Note periodic variation of the thickness of the odd and even numbered lines of laser-induced crystal as a result of different penetration depths of the laser beam in glass and crystal regions.

With regard to the mechanism of lattice rotation, we suggest that the present 2D crystal contains tilt dislocation walls (TDW) as in small angle grain boundaries or disclinations, and unpaired dislocations, in analogy to 1D RLS crystal line[11]. A TDW produces small abrupt rotations ($<1^0$), while unpaired dislocations introduce gradual rotation of crystal lattice. In RLS crystal lines these dislocations and disclinations have a line vector which is parallel to the front of crystallization and sample surface, or in other words - normal to the laser scanning direction. It is the same as the direction of the Frank pseudo-vector ω for disclinations or Burger vector for dislocations. In the case of 2D crystal, the laser beam follows complex trajectory, for example, including straight line along *x*-direction, and then turns to orthogonal *y*-direction followed by another straight line, etc. In simple terms, the 2D crystal grows with dislocations and disclinations, which reproduce the trajectory of laser beam and help relax interfacial stresses at the growth front most efficiently (see Figures 8-11).

CONCLUSIONS

We have demonstrated the feasibility of fabricating 2D single crystal architecture from glass by an all-solid-state single crystal growth process. Two different protocols, 'stitching' and 'rastering', were designed and tested for the fabrication of simple 2D patterns by combining single crystal lines. The former requires new nucleation event at the end of each line and growth only in straight line, whereas the latter starts with one nucleus and continues with a zig-zag growth pattern. It was found for the 'stitching' protocol that if the step between successive lines is larger than half the width of the crystal line, the new crystal line can have orientation different from that of the preceding crystal line. However, if the step width is less than half the width of the crystal line, a 2D RLS crystal is obtained. Compared to stitching, the rastering protocol appears more promising, in which case a 2D crystal can be formed with only 1-2 μm overlap between successive lines. For materials that may decompose/evaporate on heating, wide single crystal lines can be made by decreasing the laser power density by increasing the laser beam size, for instance, by shifting the focus of the laser beam a few microns above the surface of glass sample.

For the investigated Sb_2S_3 crystal pattern on the surface of $16SbI_3$–$84Sb_2S_3$ glass, the rate of lattice rotation is determined by the direction of laser movement relative to initial lattice orientation. So, an appropriate choice of initial seed orientation and direction of scanning can help minimize the rate of lattice rotation, for example, down to 5^o for a 2D pattern of 50x50 μm^2 size.

All lines of 2D patterns created by both protocols demonstrate strongly correlated rotation, which is determined by rotation of the first line. The PF maps obtained from the analysis of

μSXRD Laue patterns show that the rotation within all lines have a component that parallels those in an isolated RLS crystal line. In addition, there is also an orthogonal component of rotation, which depends on the extent of overlap between successive lines, and can be different for the two protocols. Finally, the odd and even-numbered lines in either protocol may have different additional orthogonal component of rotation, presumably due the difference between optical absorption of the laser light by glass matrix and growing crystal.

AUTHOR INFORMATION

Corresponding Author

*E-mail: h.jain@Lehigh.EDU

Author Contributions

D.S., V.D. and H.J. designed the overall research, and interpreted results; D.S. and C.A. prepared the samples, designed and implemented characterization methods and analyzed results; N.T. designed scanning Laue X-ray microdiffraction (μSXRD) setup and analyzed results; H.J., V.D. and D.S. wrote the paper.

Funding Sources

This work was supported by the Basic Energy Sciences Division, Department of Energy (DE-SC0005010). C. Au-Yeung, who helped with EBSD analysis, was supported by National Science Foundation and Lehigh University. The Advanced Light Source is supported by the Director, Office of Science, Office of Basic Energy Sciences, Materials Sciences Division, of the U.S.

Department of Energy under Contract No. DE-AC02-05CH11231 at Lawrence Berkeley National Laboratory and University of California, Berkeley, California.

Notes

The authors declare no competing financial interest.

ACKNOWLEDGEMENT

The authors thank B. Knorr for help with the laser control, and S. McAnany and C. Stan for assistance with the μSXRD experiments.

ABBREVIATIONS

RLS crystal, Rotating lattice single crystal; EBSD, Electron Backscatter Diffraction; μSXRD, scanning Laue X-ray microdiffraction; SCAG, single-crystal architecture in glass; CW, Continuous Wave; fs, femtosecond; Tx, temperature of crystallization; Tm, melting temperature; SEM, Scanning Electron Microscope; OIM, Orientation imaging microscopy; IPF, Inverse Pole Figure; ND, Normal Direction; RD, Rolling Direction; TD, Transverse Direction; COD map, Crystal orientation deviation map; PFM, Pole figure map; TDW, tilt dislocation walls.

REFERENCES

1. Komatsu, T., Ihara, R., Honma, T., Benino, Y., *J. Am. Ceram. Soc.* **2007**, *90*, 699-705.

2. Stone, A. *et al. Sci. Rep.* **2015**, *5*, 10391.

3. Fan, C., Poumellec, B., Lancry, M., He, X., Zeng, H., Erraji-Chahid, A., Liu, Q., Chen, G. *Opt. Lett.* **2012**, *37*, 2955-2957.

4. Komatsu, T., Honma, T. *J. Asian Ceram. Soc.*, **2013**, *1 (1)*, 9–16.

5. Arun, P., Vedeshwar, A.G., Mehra, N.C. *J. Phys. D: Appl. Phys.* **1999**, *32*, 183–190.

6. Gupta, P., Stone, A., Woodward, N., Dierolf, V., Jain, H. *Opt. Mater. Exp.* **2011**, *1***,** 652-657.

7. Savytskii, D., Knorr, B., Dierolf, V., Jain, H. *Sci. Rep.*, **2016**, *6*, 23324.

8. Honma, T., Komatsu, T. *Opt. Express*, **2010**, *18*, 8019.

9. Suzuki, F., Ogawa, K., Honma, T., Komatsu, T. *J. Sol. State Chem.*, **2012**, *185*, 130-135.

10. Suzuki, F., Honma, T., Komatsu, *Mater. Chem. Phys*., **2011**, *125*, 377-381.

11. Savytskii, D., Jain, H., Tamura, N., Dierolf, V. *Sci. Rep.*, **2016**, *6*, 36449.

12. Varghese, J., Barth, S., Keeney, L., Whatmore, R. W., Holmes, J. D. *Nano Lett.* **2012,** *12*, 868–872.

13. Savytskii, D., Atwater, K., Dierolf, V. and Jain, H. *J. Am. Ceram. Soc.*, **2014**, *97*, 3458-3462.

14. Savytskii, D., Knorr, B., Dierolf, V., Jain, H. *J. Non-Cryst. Solids* **2016**, *431*, 36-40.

15. Savytskii, D. Knorr, B. Dierolf, V. Jain, H. *J. Non-Cryst. Solids* **2013**, *377*, 245–249.

16. Savytskii, D., Knorr, B., Dierolf, V., Jain, H. *Opt. Mater. Exp.* **2013**, *3*, 1026-1038.

17. http://www.edax.com/Products/EBSD/OIM-Data-Analysis-Microstructure-Analysis.aspx

18. Kunz, M., *et al.* E. *Rev. Sci. Instrum.* **2009**, *80*, 035108.

19. Tamura, N. In *Strain and Dislocation Gradients from Diffraction. Spatially Resolved Local Structure and Defects*; Barabash, R., Ice, G. Eds.; Imperial College Press, London, 2014; chapter 4, pp 125-155.

20. Palache, C. Berman, H. Frondel, C. In *The System of Mineralogy*; John Willey and Sons, New York, ed. 7, 1944; Vol.1, pp 270-275.

21. Scavnicar, S. *Z. Kristallogr.* **1960**, ***114***, 85-97.

22. Bayliss, P. Nowacki, W. *Z. Kristallogr.* **1972**, *135*, 308-315.

FOR TABLE OF CONTENTS USE ONLY:

FIGURE:

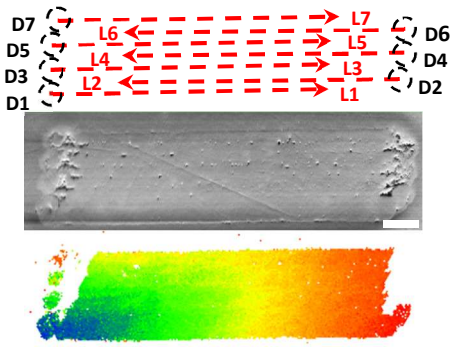

SYNOPSIS:

The nature of lattice rotation within 2D RLS crystals is established for the first time using Sb_2S_3 as model compound, which is fabricated on the surface of $16SbI_3$–$84Sb_2S_3$ glass by 'stitching'

multiple lines or ‘rastering’ a single line. The electron back scattered diffraction mapping and scanning Laue X-ray microdiffraction of such a 2D RLS crystal show gradual rotation of lattice comprising of two components, one along the length of each line and another normal to this direction.